Paths in the minimally weighted path model are incompatible with Schramm-Loewner evolution

C. Norrenbrock,* O. Melchert,† and A. K. Hartmann‡
Institut für Physik, Universität Oldenburg, 26111 Oldenburg, Germany
(Received 11 May 2012; revised manuscript received 29 January 2013; published 20 March 2013)

We study numerically the geometrical properties of minimally weighted paths that appear in the minimally weighted path (MWP) model on two-dimensional lattices assuming a combination of periodic and free boundary conditions (BCs). Each realization of the disorder consists of a random fraction $(1-\rho)$ of bonds with unit strength and a fraction ρ of bond strengths drawn from a Gaussian distribution with zero mean and unit width. For each such sample, a path is forced to span the lattice along the direction with the free BCs. The path and a set of negatively weighted loops form a ground state. A ground state on such a lattice can be determined performing a nontrivial transformation of the original graph and applying sophisticated matching algorithms. Here we examine whether the geometrical properties of the paths are in accordance with the predictions of the Schramm-Loewner evolution (SLE). Measuring the fractal dimension, considering the winding angle statistics, and reviewing Schramm's left passage formula indicate that the paths cannot be described in terms of SLE.

DOI: 10.1103/PhysRevE.87.032142 PACS number(s): 64.60.ah, 75.40.Mg, 02.60.Pn, 68.35.Rh

I. INTRODUCTION

The statistical properties of lattice-path models on graphs, often equipped with quenched disorder, have experienced much attention during the last decades. Such paths can be as simple as the boundaries of percolation clusters [1] or domain walls in planar Ising systems [2]. Beyond this, they have proven to be useful to describe more complex line-like quantities as, e.g., linear polymers in disordered media [3–6], vortices in high T_c superconductivity [7,8], cosmic strings in the early universe [9–11], and domain-wall excitations in disordered systems such as $2d$ spin glasses [12,13] and the $2d$ solid-on-solid model [14]. So as to analyze the statistical properties of these lattice path models, geometric observables and scaling concepts similar to those used in percolation theory [1,15] or other string-bearing models [16,17] are often applicable. Recently, the question of which of these path models can be described in terms of the Schramm-Loewner evolution (SLE) [18–21] has attracted much attention.

Basic problems like polymers and domain walls in Ising systems can be treated numerically by standard approaches [1,22]. For more complex models this is not straightforward. Nevertheless, the precise computation of these paths can often be formulated in terms of a combinatorial optimization problem and hence might allow for the application of exact optimization algorithms developed in computer science [23,24].

In this article we study paths in the minimally weighted path (MWP) model [25], which is related to a similar model called "negative-weight percolation" in previous publications. The basis of this model is given by a weighted, undirected, d-dimensional lattice graph with side length L where the weights are assigned to the edges taken from a distribution that allows for the values of either sign. For a given realization of the disorder, a configuration consisting of one path, spanning the lattice along the direction of the free boundaries (the path extremities are forced to lie on the free boundaries), and possibly a set of loops, i.e., closed paths, can be found such that the loops and the path do not intersect one another and the total sum of the weights assigned to the edges which build up this configuration attains an *exact* minimum. The fraction of negatively weighted edges can be controlled by a tunable disorder parameter ρ that gives rise to qualitatively different ground states as depicted in Fig. 1.

As presented here, the MWP problem is a theoretical model of intrinsic interest. As an example that makes use of the statement of the MWP problem, an agent can be imagined that travels on a graph. While traversing an edge, the agent either needs to pay some resource (signified by a positive edge weight) or is able to harvest some resource (signified by a negative edge weight). To gain as many resources as possible, the path or loops obtained in the context of the MWP problem serve as a guide to find optimal routes.

The problem of detecting the exact minimum-weight configuration for a given realization of the disorder becomes solvable through a mapping of the original graph to the minimum-weight perfect-matching optimization problem as outlined in Sec. II. This mapping allows for applying exact polynomial-time-running algorithms, thus large instances can be solved. Note that the same mapping and algorithms can be used in the context of finding ground-state spin configurations for the planar triangular random-bond Ising model since this problem is equivalent to the MWP problem on a planar honeycomb lattice [26,27].

In a previous study it was shown that the MWP model features a disorder-driven geometric phase transition [25]. Depending on the disorder parameter, two distinct phases can be identified: (i) a phase where the loops (if there are any) are small and the shape of the path is rather straight-lined, reflecting a self-affine scaling of the path length [cf. Fig. 1(a)] and (ii) a phase where large loops emerge and the extension of the horizontal projection of the path is $O(L)$, reflecting a self-similar scaling of the path length [cf. Fig. 1(c)], i.e., the path winds around the lattice. If there are many negatively weighted edges in the lattice, it will become profitable for the paths to increase in length to include many negative-weighted

*christoph.norrenbrock@uni-oldenburg.de
†oliver.melchert@uni-oldenburg.de
‡alexander.hartmann@uni-oldenburg.de

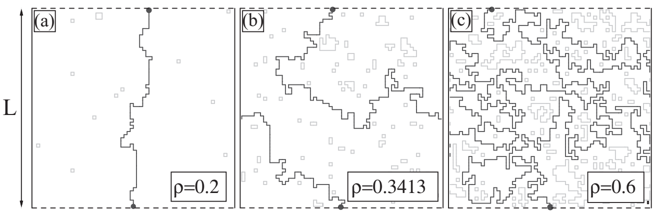

FIG. 1. Illustration of minimum-weight configurations consisting of loops (gray) and one path (black) in a regular 2D square lattice of side length $L = 64$. The boundary conditions are periodic in horizontal (left-right) direction and free in vertical direction. The path is forced to connect the middle of the lower boundary to the upper boundary. The minimum-weight configurations minimize Eq. (3). For a small value of the disorder parameter $\rho = 0.2$, the path crosses the lattice in a rather straight fashion since the path weight is mainly determined by its length. Increasing the order parameter to $\rho = 0.3413$, the path length increases as well and the path takes advantage of more negative-weighted edges. If the disorder parameter is increased to $\rho = 0.6$, the loops and the path will become more dense.

edges. Hence, it will be beneficial for the paths to take some "detours," which will be reflected by the scaling behavior of the path length. The opposite would be true if all edges were positively weighted, so an increasing path length would be payed off by an increasing configurational weight of the path. Consequently, the path would gather as few edges as possible to minimize its configurational weight. Furthermore, the loops could not appear since they would always increase the weight of the combined path + loops configuration. In this later limit, the complete problem would be changed to a standard shortest-path problem as is used to study polymers in disordered media. Such polymers are never self-similar, but self-affine. On the other hand, in the limit of large system sizes in the MWP model, there is a particular value of the disorder parameter, i.e., the critical point, at which the path simultaneously spans the lattice along both directions for the first time [cf. Fig. 1(b)]. For two-dimensional (2D) lattice graphs, the respective disorder-driven phase transition was investigated using finite-size scaling analyses and characterized by a set of critical exponents. It turned out that the exponents were universal in 2D (different disorder distributions and lattice geometries were studied). Regarding loops only, the influence of dilution on the critical properties of the 2D MWP phenomenon was investigated in a subsequent study [28]. In a further study, the upper critical dimension d_u of the MWP model was searched for by performing simulations on hyper-cubic lattice graphs in dimensions $d = 2$ through 7 [29] and evidence was found for an upper critical dimension $d_u = 6$. In contrast to that, another upper critical dimension $d_u^{\mathrm{DPL}} = 3$ was determined for densely packed loops which appear if the disorder parameter is far above the critical point that indicates the phase transition [30]. Only recently, the mean-field behavior of the MWP model was investigated on a random graph with fixed connectivity [31]. By means of numerical simulations as well as an analytic approach (using the replica symmetric cavity method for a related polymer problem), the location of the phase transition and the values of the critical exponents were determined.

Here we study the geometrical properties of MWPs connecting opposite (free) boundaries in the 2D MWP model at the critical point. To be more precise, we find the answer to the question whether these paths belong to the particular family of planar curves that can be described in terms of SLE [18–20]. The (chordal) SLE formulation describes a self-avoiding curve γ_t ("time" $t \in \mathbb{R}^+$) in the upper half plane $\mathbf{H}$, which is equivalent to any other simply connected planar domain by conformal invariance. The curve γ_t grows dynamically from the origin to infinity with time t. A conformal mapping $g_t(z)$ ($z \in \mathbb{C}$ corresponding to the 2D plane) maps the complement of the set consisting of γ_t plus all points that are not reachable from infinity without crossing γ_t, i.e., the hull, to the upper half plane at each infinitesimal time step. Thus, the boundary between the reachable and unreachable points is mapped on the real axis and $g_t(z)$ maps the growing tip successively to a real point a_t. As a consequence, a_t moves continuously on the real axis during the growing process. Then the time-evolution of $g_t(z)$ satisfies an ordinary differential equation, also referred to as a Loewner equation

$$\frac{dg_t(z)}{dt} = \frac{2}{g_t(z) - a_t}. \tag{1}$$

If a_t is proportional to a one-dimensional Brownian motion $\sqrt{\kappa}B_t$, which is a stochastic Markov process, the resulting curve will be conformal invariant [32] and the evolution will be referred to as SLE. Consequently, an ensemble of curves that can be described in terms of SLE is characterized and classified by just one parameter, the so-called *diffusion constant* κ. In the last decade, a lot of physical systems have been studied in the context of SLE.

To name but a few, boundaries of vorticity clusters in 2D turbulence ($\kappa = 6$) [33], spin cluster boundaries in the Ising model at the critical temperature ($\kappa = 3$) [34], and critical percolation ($\kappa = 6$) [35] fall into the classification scheme of SLE. Numerical evidence [36] indicates that also 2D spin-glasses can be described in terms of SLE. A detailed introduction and many results concerning SLE (in particular for disordered lattice-models) were published in [37]. In contrast to the examples mentioned above, it will be shown in this article that paths in the MWP model cannot be described by SLE.

The remainder of the presented article is organized as follows. In Sec. II, we introduce the model in more detail and outline the algorithm used to compute the minimum-weight configurations consisting of loops plus one path. In Sec. IV, we describe two measuring techniques for determining the diffusion constant and present the results of our numerical simulations. In Sec. V we conclude with a summary. Note that an extensive summary of this paper is available at the *papercore database* [38].

II. MODEL

In this article we study 2D square lattice graphs $G = (V,E)$ with both rectangular and circular shape. In this section, we first discuss the model of negative-weight paths for arbitrary graphs G. Next, we specify the different lattice geometries, i.e., the types of graphs we consider.

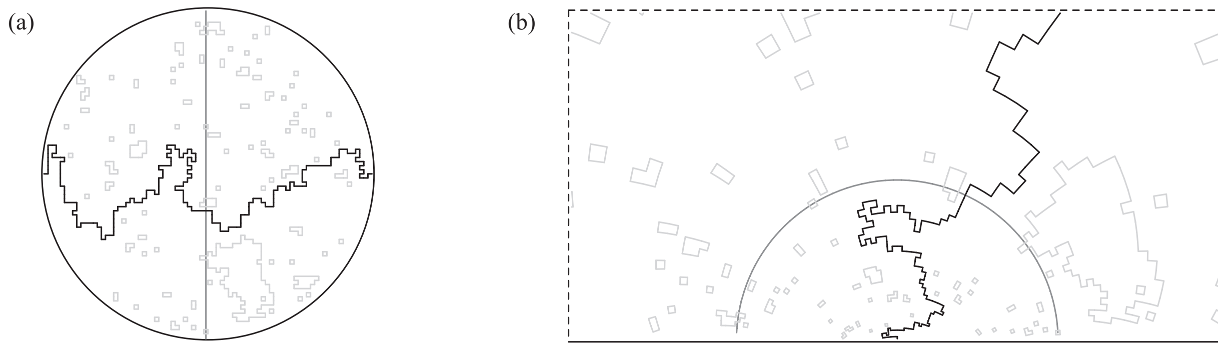

FIG. 2. (a) Illustration of a minimum-weight configuration consisting of loops (gray) and one path (black) in the unit disk with a radius of 40. The terminal points of the path are fixed on $-1 + 0i$ and $1 + 0i$ to ensure that they will be mapped as required by Cayley's function. All points which Schramm's left passage formula is checked for are located on the vertical solid line (deep gray). (b) The same minimum-weight configuration as in (a) after the conformal mapping by Cayley's function has been performed, so the path connects the origin to infinity in the upper half plane. The dashed lines indicate that the lattice is not displayed completely. Due to the mapping, the original, vertical line containing all checkpoints becomes a semicircle.

A. Model definition

We assign a weight ω_{ij} to each edge contained in E. These weights represent quenched random variables that introduce disorder to the lattice and are drawn from a distribution that allows for values of either sign. In the presented article the edge weights are taken from a "Gauss-like" distribution characterized by a tunable disorder parameter ρ

$$P(\omega) = (1-\rho)\delta(\omega-1) + \rho\exp(-\omega^2)/\sqrt{2\pi}, \quad 0 \leqslant \rho \leqslant 1. \tag{2}$$

This weight distribution explicitly allows for loops $\mathcal{L}$ with the negative weight given by $\omega_{\mathcal{L}} \equiv \sum_{\{i,j\}\in\mathcal{L}} \omega_{ij}$. In addition one path $\mathcal{P}$ is forced on the lattice whose endpoints lie on the horizontal boundaries. One endpoint is fixed at the central node of the lower boundary, hence, the starting point of the path is predetermined, and the other end terminates at a site at the top boundary determined by the optimality criterion given below, hence, the endpoint of the path is not predetermined. Moreover, the loops and the path are not allowed to intersect each other, hence every edge is contained in at most one loop (or path). Given a realization of the disorder, the exact geometrical configuration $\mathcal{C}$ of loops and one path is determined by the following criterion: The configurational energy $\mathcal{E}$ defined as

$$\mathcal{E} = \sum_{\mathcal{L}\in\mathcal{C}} \omega_{\mathcal{L}} + \omega_{\mathcal{P}} \tag{3}$$

has to be minimized, where $\omega_{\mathcal{P}}$ denotes the total of all edge weights belonging to the path. Such minimum-weight configurations for different values of the disorder parameter are presented in Fig. 1.

B. Geometries

In principle, one would like to simulate the MWP on the upper half plane, i.e., on an infinite system, which is not feasible. Hence, we considered different finite-size approximations of the upper half plane.

On the one hand, we approximate the upper half plane directly by constructing a rectangular lattice featuring appropriate boundary conditions. The top and bottom boundaries of a rectangular lattice graphs are chosen to be free and the left and right ones are periodic, i.e., the considered lattices are cylindrical. The system size $L = L_y$ denotes the number of nodes in the vertical direction. As justified in Sec. IV the number of nodes in the horizontal profile corresponds to $L_x = 4L + 1$. Thus the considered graphs have $N = |V| = L(4L + 1)$ sites $i \in V$ and a number of $|E| = (2L - 1)(4L + 1)$ undirected edges $\{i,j\} \in E$ that join the adjacent sites $i,j \in V$.

On the other hand, we design a square lattice exhibiting a circular contour and regard it as unit disk $\mathbf{E}$ in the complex plane. The unit circle can be mapped conformally into the upper half plane by a simple mapping called the Cayley function [39]

$$g : \mathbf{E} \to \mathbf{H}, \qquad z \mapsto i\,\frac{1+z}{1-z}. \tag{4}$$

The mapping provides $g(-1) = 0$ and $g(1) = \infty$, thus a curve in $\mathbf{E}$ linking $-1 + 0i$ and $1 + 0i$ is mapped by g as required. For a given realization of the disorder, the ground state in the unit disk and the corresponding ground state in the upper half plane are illustrated in Fig. 2 to support intuition.

III. ALGORITHM

To get over that "minimum-weight configuration problem" Eq. (3) we transform the original graph as detailed in [40] to an appropriate auxiliary graph and detect a *minimum-weight perfect matching* (MWPM) [26,41,42] subsequently. Here, we give a concise description of the algorithmic procedure illustrated in Fig. 3 for a given realization of the disorder (for clarity without periodic boundary conditions).

(1) To force a path that satisfies the specified boundary conditions, two "extra" nodes are added in the following way: One extra node is linked to the node located in the center of the lower boundary and the other extra node is connected to all nodes at the upper boundary [cf. Fig. 3(b)]. All added edges get zero weight.

(2) Each edge is replaced by two "additional" nodes and three edges which are arranged in a row as depicted in Fig. 3(c). Therein, one of the two edges connecting an additional node

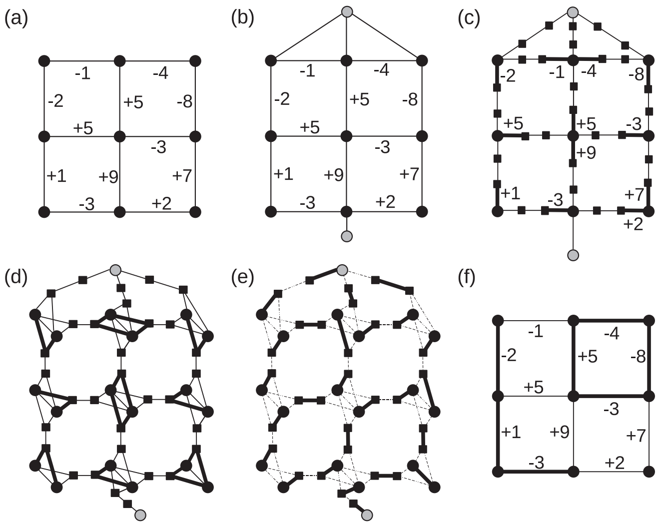

FIG. 3. Illustration of the algorithmic procedure: Illustrated edges that are not marked by a weight visually carry a zero weight actually [except in (d) and (e)]. (a) The initial, weighted lattice graph. (b) Two extra nodes (gray) are added to render a path possible. They are connected to the lattice boundaries as described in the text. (c) Each edge is replaced by two nodes (black boxes) and three edges joining the original nodes and the added nodes in a row. The initial weights are assigned to one of the added edges (bold edges) that join one of the original nodes and one extra node. (d) The original nodes are duplicated preserving their neighbors. Additionally, the duplicated nodes are interconnected by an added edge carrying a zero weight. (e) A MWPM is computed: Bold edges are matched and dashed ones are unmatched. (f) Reconstruction to the initial lattice taking the MWPM result into account. The thickly denoted path and loop represent the minimally weighted configuration.

to an original node gets the same weight as the corresponding edge in the original graph G. The remaining two edges get zero weight.

(3) Subsequently, the original nodes $i \in V$ (i.e., not the two extra nodes) are "duplicated," i.e., $i \rightarrow i_1, i_2$, along with all their incident edges and the corresponding weights. For each of these pairs of duplicated nodes, one edge $\{i_1, i_2\}$ with zero weight is added that connects the two nodes i_1 and i_2. The resulting auxiliary graph $G(V_A, E_A)$ is illustrated in Fig. 3(d) without showing the edge weight assignment for reasons of clarity. Note that while the original graph is symmetric, the transformed graph is not. This is due to the details of the mapping procedure and the particular weight assignment we have chosen. A more extensive description of the mapping (in terms of minimum-energy domain wall calculations for the 2D Ising spin glass) can be found in [13].

(4) A MWPM on the auxiliary graph is determined via exact combinatorial optimization algorithms [43]. A MWPM is a minimum-weighted subset M of E_A, such that each node contained in V_A is met by precisely one edge in M. This is illustrated in Fig. 3(e), where the solid edges represent M for the given weight assignment. The dashed edges are not matched. Due to construction, the auxiliary graph consists of an even number of nodes and due to the fact that pairs of duplicated nodes are connected by additional edges (see step 3), it is guaranteed that a perfect matching exists.

(5) Finally it is possible to find a relation between the matched edges M on G_A and a minimally weighted configuration consisting of loops and one path in G by tracing back the steps of the transformation. As regards this, note that each edge contained in M that connects an additional node (square) to a duplicated node (circle) corresponds to an edge in G that is part of a loop or path, see Fig. 3(f). More precisely, there are always two such edges in M that correspond to one loop or path segment on G. All the edges in M that connect like nodes (i.e., duplicated-duplicated or additional-additional) carry zero weight and do not contribute to the minimally weighted configuration and correspondingly do not belong to loops or to the path in the original graph. Once such a configuration is found, a depth-first search [40,42] can be used to identify the path and to determine its geometrical properties. For the weight assignment illustrated in Fig. 3(a), the path features $\omega_p = -4$ and length $\ell = 3$.

It is important to emphasize that the result of the calculation is a collection $\mathcal{C}$ of loops and one path, such that their total weight, and consequently the configurational energy $\mathcal{E}$, is minimized. Hence, one obtains a global collective optimum. This implies that the weight of the resulting path might not be its absolute minimum: Due to the no-crossing condition, the loops might affect its precise location. While all the loops that contribute to $\mathcal{C}$ possess a negative weight, the weight of the path might be positive as well. The set of loops might be empty, but the addition of the two extra nodes during the first step of the mapping outlined above ensures that the solution of the auxiliary minimum-weight perfect matching problem always yields (at least) a path.

Note that the choice of the weight assignment in step 2 is not unique, i.e., there are different ways to choose a weight assignment that all result in equivalent sets of matched edges in the transformed lattice, corresponding to the minimum-weight configuration in the original lattice. Some of these weight assignments result in a more symmetric transformed graph (see, e.g., [40]). However, this is only a technical issue that does not affect the result.

IV. RESULTS

As pointed out in the Introduction, we aim at finding an answer to the question whether paths in the MWP model can be described in terms of SLE at the critical point, and, if so, which value of κ characterizes these paths.

The critical point $\rho_c = 0.3413(9)$ has been estimated in the same way as in [25] with slightly higher precision. Principally, SLE curves can be calculated by Eq. (1). This stochastic differential equation does not provide a unique curve for a given diffusion constant κ, but provides a set of curves that exhibits particular properties in a statistical sense. These properties can be utilized to approach the question whether a given ensemble of curves is a potential candidate for showing SLE. Hence, below we are showing the results for different ways of calculating κ. As mentioned in the Introduction, the paths in the MWP model turned out to be not consistently described by SLE, as different value of κ result. Therefore, we also address the question whether MWP is conformal invariant right in the next section.

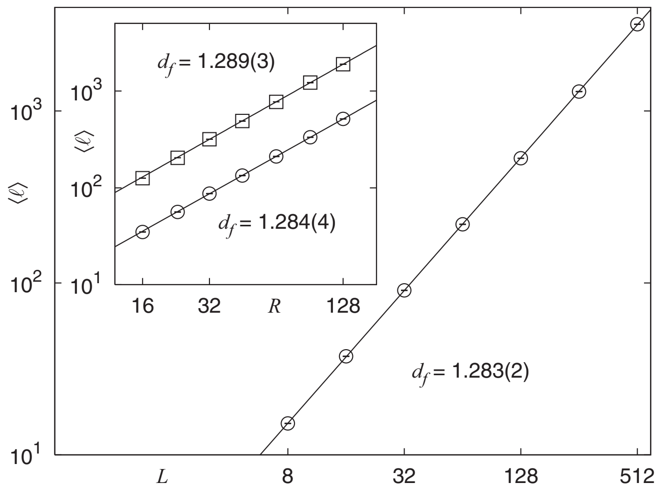

FIG. 4. Estimation of the fractal dimension d_f by means of a simple fit to the power-law data. The data points were obtained by measuring the averaged path length $\langle\ell\rangle$ on a square lattice scale 4 : 1. The inset also shows estimation of the fractal dimension obtained by measuring $\langle\ell\rangle$ on the unit disk (circles) and by considering paths on the upper half plane (boxes) that have been created on the unit disk first and mapped [with Eq. (4)] to the upper half plane subsequently. R describes the number of nodes which discretize the radius of the unit disk. Note that the upper dataset was shifted vertically for a more clear presentation. As a matter of fact, the circles and boxes almost lie on top of each other.

A. Value of κ from fractal dimension

The first property takes the fractal dimension d_f into account. The fractal dimension can be defined from the scaling of the average length $\langle\ell\rangle$ of the paths as a function of the system size L, according $\langle\ell\rangle \sim L^{d_f}$. In the context of SLE there is a relation between the diffusion constant and the fractal dimension [44,45]

$$\kappa = 8(d_f - 1), \quad \kappa \leqslant 8. \tag{5}$$

The fractal dimension is fixed at $d_f = 2$ for $\kappa > 8$.

We measured the average path length for seven different system sizes on the rectangular geometry as a function of the path length. Each data point is generated by means of 12 800 realizations of the disorder. A simple fit to the power-law data shown in Fig. 4 yields the exponent $d_f = 1.283(2)$, but due to our high statistical accuracy, only a mediocre quality of fit. When restricting the fit to sizes $L > 64$ the quality of fit is acceptable, with a result $d_f = 1.288(4)$ still being compatible with the result from the full fit. We also tried an estimation by extrapolation using local effective exponents [46], but since the number of different system sizes is not large, this results in a larger error bar, i.e., $d_f = 1.27(9)$, hence we did not take this result into account. According to Eq. (5), the estimate with the best fit quality yields $\kappa = 2.30(4)$.

To test conformal invariance, we also measured the fractal dimension of paths on the unit disk and paths that have been mapped to the upper half plane. As can be seen from Fig. 4 (upper inset), both estimates agree well, $d_f = 1.289(3)$ and $d_f = 1.284(4)$, respectively, and also with the above result. This provides numerical evidence that conformal invariance is satisfied in the MWP model.

B. Value of κ from left passage formula

Similar to [14,47–50] we examine the predictions of Schramm's left passage formula (SLPF) to obtain a second estimation for κ. As proven in [51]

$$P_\kappa(z) = \frac{1}{2} + \frac{\Gamma(4/\kappa)}{\sqrt{\pi}\,\Gamma((8-\kappa)/2\kappa)} \times {}_2F_1\left[\frac{1}{2},\frac{4}{\kappa};\frac{3}{2};-\left(\frac{x}{y}\right)^2\right]\frac{x}{y} \tag{6}$$

yields the probability that a curve which can be described in terms of SLE will pass to the left of a given point $z = x + iy$ in the upper half plane provided that the curve links the origin to infinity. ${}_2F_1$ denotes the Gaussian hypergeometric function and Γ the gamma function. $P_\kappa(z)$ does not depend on the distance between the origin and point z. Thus the ratio between $\mathrm{Re}(z)$ and $\mathrm{Im}(z)$ can be replaced by a function of an angle. A proper angle $\phi \in [-\pi/2,\pi/2]$ between the imaginary axis and the reference point z is located in the origin of the upper half plane as depicted in Fig. 5(b) [14]. Thus the ratio between x and y is given by $x/y = \tan\phi$. A curve γ will be considered as passing to the left of a given point z if there exists a continuous path between z and the positive real axis that does not intersect γ [52]. To support intuition, Fig. 6 shows the SLPF for a particular value of κ (at this point the reference to the figure is only meant to illustrate the general functional form of the SLPF, the precise value of the parameters ρ and κ and the results implied by them are discussed below).

Note that Eq. (6) holds in the upper half plane only. Subsequently we consider two different lattice geometries that aim to approximate the upper half plane.

First we consider the rectangular lattice shape. To approximate the upper half plane as accurately as possible, the terminal points of the paths in the MWP model are chosen as described in Sec. II. The terminal point located at the central node of the lower boundary is considered as the origin of the coordinate system. Furthermore, all considered lattices are on a scale of 4 : 1 to avoid the influence of the finite size in the horizontal direction. An example of a minimally weighted configuration in such a lattice is shown in Fig. 5(a) for a lattice of size 257×64. Although SLPF applies for all points in the upper half plane, its predictions are often checked for properly chosen points only. Aside from κ, Eq. (6) depends on angle ϕ merely, thus it is sufficient to consider points located on a semicircle, whose central point is located in the origin of the upper half plane. The distance between the center of this semicircle and every point located on its boundary should be equal. For that reason and due to the "Manhattan structure" of the underlying lattice, the semicircle assumes the shape of a triangle as illustrated in Fig. 5. The path is able to cross the semicircle at particular points only. The checkpoints we consider to examine predictions of SLPF are located exactly between these possible crossing points. Each checkpoint is examined independently for a given realization of the disorder, i.e., for each given path. In so doing, for a sufficient large number of samples N_s, each checkpoint will exhibit a measured left-passage probability $p(\phi) \pm \Delta_P(\phi)$ where $\Delta_P(\phi)$ is the standard error $\sqrt{p(\phi)[1-p(\phi)]/(N_s-1)}$ [53]. A comparison between these measured probabilities $p(\phi)$ and the corresponding predictions

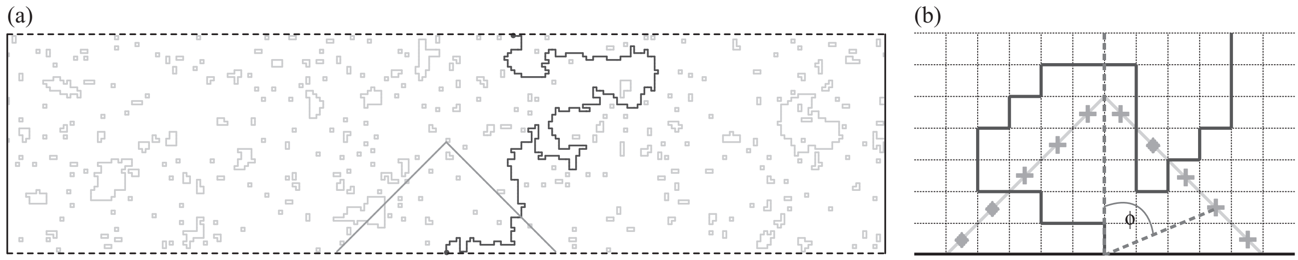

FIG. 5. (a) Illustration of a minimum-weight configuration consisting of loops (gray) and one path (black) in a lattice of size 257×64. Due to the "Manhattan-structure" of the underlying lattice, the semicircle ($R = 32$) assumes the shape of a triangle (light gray). The boundaries at the top and bottom border (dashed) are free and the ones left and right (solid) are periodic. For testing, we also considered the case where also the left and right boundaries exhibit free boundary conditions. The edge weights are taken from a "Gauss-like" distribution shown in Eq. (2) featuring $\rho = 0.3413$. The path is forced to connect the horizontal boundaries as described in the text. The minimum-weight configuration has to minimize Eq. (3). (b) Sketch of a lattice that approximates the upper half plane to check SLPF predictions at some certain places located on the semicircle. The checkpoints marked by rhombuses lie on the left and the other ones (crosses) on the right of the path (black). For every realization of the disorder, the predictions of SLPF are examined independently for each checkpoint. ϕ states the angle between the ordinate and considered checkpoints in the upper half plane.

of SLPF provides an estimate for κ. The minimum of the cumulative squared deviation

$$f_{SC}(\kappa) = \frac{1}{N_\phi} \sum_{\phi \in SC} \left[\frac{p(\phi) - P_\kappa(\phi)}{\Delta_P(\phi)} \right]^2$$

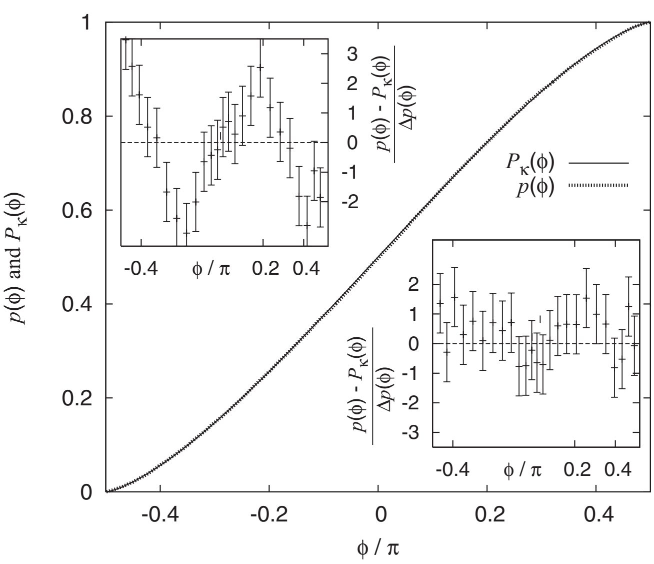

FIG. 6. Comparison between the measured probabilities $p(\phi)$ and the predictions of SLPF $P_\kappa(\phi)$. The left passage probability $p(\phi)$ has been measured for various points on a semicircle ($R = 128$). ϕ denotes the angle that is illustrated in Fig. 5 (right). The computational simulations have been performed at the critical point in a lattice of size 1025×256 using 51200 realizations of the disorder. The chosen diffusion constant $\kappa^\star = 3.343$ provides the finest agreement between $P_\kappa(\phi)$ and $p(\phi)$ (cf. Fig. 7). The right bottom inset illustrates the deviation of the measured left-passage probability from the SLE predictions. For reason of clarity, merely a few calculated data points are illustrated. As a matter of fact, $p(\phi)$ has been estimated for 257 different values of ϕ. The upper left inset displays the same deviation but for the case where the starting point of the path is no fixed, for the best-fitting value $\kappa^{\text{free}} = 2.89(15)$. The systematic significant deviations indicate that here the left-passage formula does not hold.

yields the finest agreement between $P_\kappa(\phi)$ and $p(\phi)$, where SC denotes a set containing all possible angles of the considered checkpoints and $N_\phi = |SC|$ is the size of SC. The cumulative squared deviation as a function of κ is illustrated in Fig. 7 for a lattice of size 1025×256.

In so doing $f_{SC}(\kappa)$ and its error bar $\Delta f_{SC}(\kappa)$ have been calculated for a set of $M = 4000$ individual values of $\kappa \in K$, where $K = \{\kappa_1, \kappa_2, \ldots, \kappa_M\}$. If $\kappa^\star$ denotes the diffusion constant where the squared deviation $f_{SC}(\kappa)$ is minimal, its error bar $\Delta\kappa^\star$ will be estimated as follows: Defining $\Omega = \{\kappa \in K \,|\, f_{SC}(\kappa^\star) + \Delta f_{SC}(\kappa^\star) \geqslant f_{SC}(\kappa) - \Delta f_{SC}(\kappa)\}$, one has

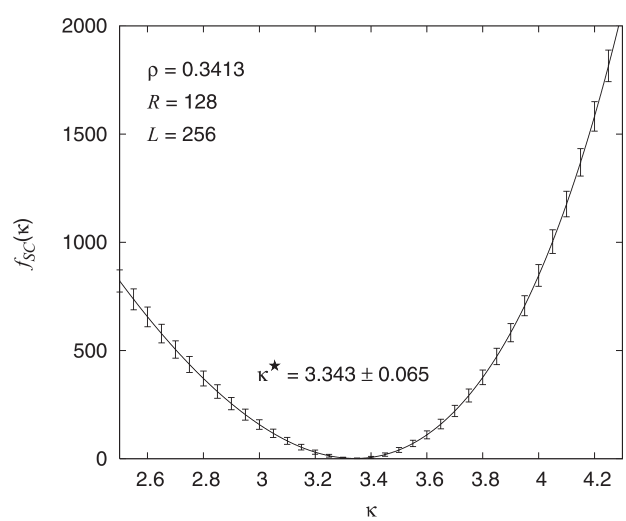

FIG. 7. The cumulative squared deviation $f_{SC}(\kappa)$ of the measured probabilities $p(\phi)$ from the corresponding values given by Schramm's left passage formula $P_\kappa(\phi)$ as a function of the diffusion constant κ. The semicircle, which contains the checkpoints, features a radius $R = 128$ in a lattice of size 1025×256. The simulations (51 200 realizations of the disorder) have been performed at the critical point. The squared deviation has been calculated for discrete values of κ between 2.5 and 4.3 with step range 0.001. For reasons of clarity only a few error bars are displayed. The cumulative squared deviation yields the finest agreement between $p(\phi)$ and $P_\kappa(\phi)$ at $\kappa^\star = 3.343 \pm 0.065$.

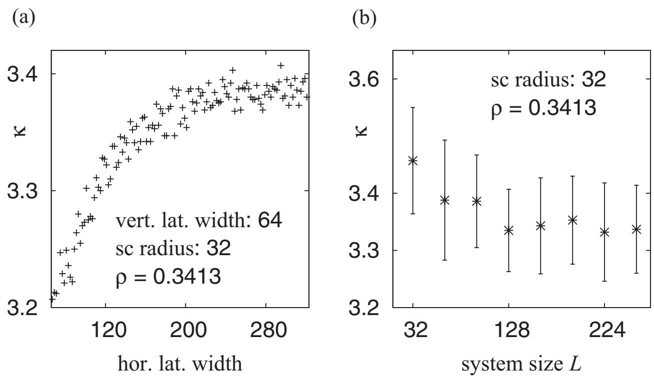

FIG. 8. (a) The diffusion constant $\kappa^\star$ depending on the ratio between the lateral extensions of the lattice. The horizontal extension L_x is varied in length and the radius R of the semicircle is chosen to be the half of the system size $L = L_y$. The estimates of the diffusion constant have been determined at the critical point by means of 51 200 realizations of the disorder. For reasons of clarity, the error bars are not illustrated. Note that all estimates (except for the shortest horizontal extensions until 80) are compatible to each other within the error bars. (b) The diffusion constant $\kappa^\star$ depending on the system size L that denotes the number of nodes in the vertical direction of the lattice. The horizontal extension is equivalent to $4L + 1$. The radius of the semicircle is chosen to be the half of the system size in every cases. The estimates of the diffusion constant have been determined at the critical point by means of 51 200 realizations of the disorder.

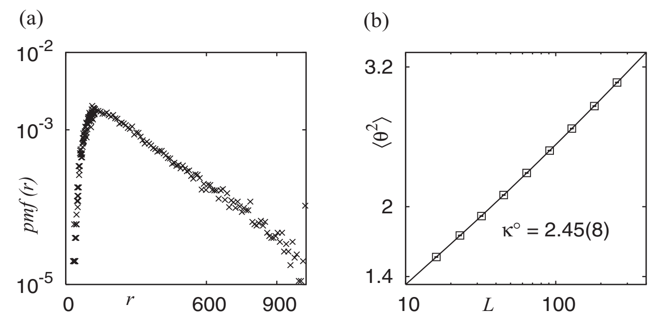

FIG. 9. (a) Probability mass function of the roughness of the paths in a lattice of size 1025×256. (b) Variance of the winding angle over the vertical width of the system. The lines indicate the result of the fit to Eq. (7), yielding $\kappa^\circ = 2.45(8)$. The error bars are smaller than the symbol size. Both the data in (a) and each data point in (b) were obtained by considering 50 000 different paths.

$\Delta\kappa^\star = \max\{|\kappa^\star - \kappa| \,|\, \kappa \in \Omega\}$. This results in $\kappa^\star = 3.343 \pm 0.065$. For checking the influence of the boundary conditions, we performed the same study for the case where the left and right borders have free boundary conditions, i.e., free boundary conditions everywhere, and obtained $\kappa^\star = 3.34 \pm 0.08$, compatible with the previous result. One also might wonder whether the result is affected by different lattice-size effects, which we consider now.

As mentioned above, we design the underlying lattice on scale of 4 : 1 to approximate the upper half plane. It is evident from Fig. 8(a) that this ratio is sufficient. We estimate the diffusion constant using the squared deviation technique described above for different aspect ratios. In doing so we fixed the number $L_y = L$ of nodes in the vertical direction and varied the horizontal extension L_x. It becomes apparent that the diffusion constant does not vary significantly above a horizontal extension that is four times bigger than the vertical extension of the lattice, in particular, all values are clearly different from the value corresponding to the fractal dimension. We also consider the probability mass function of the roughness of the paths in such a lattice, see Fig. 9(a). It turns out that the horizontal extension of the vast majority of paths is considerably smaller than the lattice width. Only a fraction 0.056 of the paths have an extension larger than $L_x/2$ and even much less get close to the system size, as is visible from the figure. Therefore we suppose that the vertical boundaries have almost no effect on the path shapes.

To receive an impression of the influence of the finite-size effects, we varied the system size L (using the 4 : 1 aspect ratio) as depicted in Fig. 8(b). Bear in mind that the system size L corresponds to the number of nodes in the vertical lattice direction. It becomes apparent that the diffusion constant estimated by using the squared deviation technique is steady sufficiently atop $L = 128$. A further study, which is not illustrated here, reveals that $\kappa^\star$ does not vary significantly for differently chosen radii of the semicircle.

Thus a good approximation to the upper half plane is provided by a lattice of size 1025×256 in addition to a semicircle with radius $R = 128$. So we estimated κ for such a lattice by examining SLPF predictions. As mentioned above, the cumulative squared deviation $f_{SC}(\kappa)$ of $p(\phi)$ and $P_\kappa(\phi)$ at ρ_c yields $\kappa^\star = 3.343(65)$ (cf. Fig. 7). A comparison to the estimate obtained from Eq. (5) [$\kappa = 2.30(4)$] reveals clearly that both estimates do not agree.

Note that for all our results shown here, the paths are fixed at the origin of (the approximations of) the upper half plane. This corresponds, e.g., for the case of checking SLE for critical ferromagnetic domains to boundary conditions where on the bottom, the left half of the spins are fixed "up" and the right half are fixed "down." We also performed tests for the rectangular geometry, where we allowed the path to start everywhere on the lower bottom. For this case, the numerical data fitted the left-passage formula much worse (see the upper left inset of Fig. 6). Anyway, for the best fit, we obtained $\kappa^{\mathrm{free}} = 2.89(15)$, which is also not compatible with the value obtained from the measurement of the fractal properties in Sec. IV A.

To ensure that this conspicuous distinction does not arise from the approximation of the upper half plane by designing a rectangular lattice, we also examine the paths on the unit disk and check the predictions of SLPF after mapping the unit disk (and, consequently, the determined ground states) into the upper half plane, as depicted in Fig. 2. The radius of the disk is discretized by 128 nodes and the terminal points of the paths are set as described above [cf. Fig. 2(a)]. Just like before, the predictions of SLPF are examined merely for checkpoints located on a semicircle [cf. Fig. 2(b)] in an analogous manner. Taking 12 800 realizations of the disorder into account, the diffusion constant $\kappa^\star = 3.34(14)$ provides the best match to the measured left-passage probability. Since this estimation of κ is equal to the estimation obtained before, it becomes apparent that the upper half plane has been approximated properly by the rectangular lattice and the estimate of κ obtained by Eq. (5) differs significantly from the estimate considering SLPF as an actual fact. Consequently, this means that paths in the MWP model cannot be described in terms of SLE.

Note that we also compared the measured left-passage probability $p(\phi)$ and the corresponding predictions of SLPF directly. From Fig. 6 it is evident that $p(\phi)$ and $P_{3.343}(\phi)$ go well together at almost all values of ϕ. Although the paths of the MWP model do not show SLE properties, the predictions of $P_{3.343}(\phi)$ appear to apply for this model at the critical point.

C. Value of κ from distribution of winding angles

Additionally we obtained a third estimate for κ by studying the winding angle statistics [54–57]. Therefore, a winding angle θ_i is assigned to each edge i along the path. Starting with edge $i = 1$ and setting $\theta_1 = 0$ (edge 1 touches the midpoint of the bottom border), the remaining winding angles can be assigned iteratively by $\theta_{i+1} = \theta_i + \alpha_i$, where α_i denotes the turning angle between edge i and $i+1$. If the paths at hand showed SLE, the variance of the distribution of all winding angles (over all edges of all paths) would scale according to $\langle\theta^2\rangle = a + (\kappa/4)\log L$, where a is a constant. We measured the variance for several system sizes from $L = 16$ to 256, see Fig. 9(b), and the slope of a simple fit through the data provides the third estimate $\kappa^{\circ,1\mathrm{st}} = 2.18(2)$, but with a poor quality of the fit ($\chi^2/\mathrm{ndf} = 14$) due to a slight curvature in the result, which is notable due to the high accuracy of our data. When allowing for power-law corrections of the form

$$\langle\theta^2\rangle = a + (\kappa/4)(\log L)(1 + cL^{-\omega}), \tag{7}$$

we obtained an extremely good quality of fit ($\chi^2/\mathrm{ndf} = 0.4$) in $\kappa^\circ = 2.45(8)$ [$a = -0.4(1)$, $c = 1.3(1)$, $\omega = 0.78(9)$], which is also not quit compatible with the result obtained using Eq. (5), but not as far away as the other estimates of κ.

To summarize, as it becomes evident from Fig. 6, Schramm's left passage formula describes the probability whether a path in the MWP model passes to the left or right of any given point in $\mathbf{H}$ correctly. Furthermore, the results obtained by Schramm's formula do not change when the paths are mapped conformally invariant from the unit disk to the upper half plane. Nevertheless, by our results, it has been excluded that the paths in the MWP model can be described by SLE, hence either conformal invariance or the Markov property [18] or both of them are not valid. Since conformal invariance seems to hold, as shown in Sec. IV A, this might indicate that the Markov property is not satisfied.

V. CONCLUSION

We examined whether paths in the MWP model fall into the classification scheme of SLE. To address this question, we studied their geometrical properties and compare them to predictions that arise from the SLE theory. First we determine the fractal dimension $d_f = 1.288(4)$ by measuring the average path length as a function of the system size. The relation $\kappa = 8(d_f - 1)$ provides an estimate for the diffusion constant $\kappa = 2.30(4)$. To get a second estimate for κ, we examined Schramm's left passage formula, which states the probability that a curve featuring particular boundary conditions and showing SLE passes to the left of a given point in the upper half plane. For this purpose we designed lattices featuring different shapes to approximate the upper half plane as sufficiently as possible. A comparison between the predictions of Schramm's formula and our numerical results provides the estimate $\kappa^\star = 3.34(8)$. Furthermore, we obtained a third estimate by considering the winding angle statistics: $\kappa^\circ = 2.45(8)$. Because of the conspicuous distinction between these estimates of κ, it became apparent that the paths in the MWP model cannot be described in terms of SLE. We propose two possible reasons for this failure of SLE for the MWP. First, the MWP from the center bottom to the top might be affected by negative loops, which arise due to the minimality criterion. The edges occupied by these loops are not available to the MWP. Nevertheless, as is visible from Fig. 1, these additional loops are small and somehow rare, hence the effect might be negligible. Note that algorithmically excluding the loops from the minimization procedure will make the problem algorithmically hard, i.e., the running time increases exponentially with the system size, such that only very small instances can be solved.

Second, the way the MWP is selected refers to a global minimization criterion, hence it cannot grow locally. Loosely speaking, the path can afford to cross a region containing few negative edges if it arrives to a region which exhibits a high concentration of negative edges as compensation. This might violate the so-called "Markov property" of SLE processes [18]. On the other hand, this argument applies only to single realizations and might be not relevant for the stochastic ensemble, which is what the SLE property describes. In fact, the domain walls in $T = 0$ 2D spin glasses are also obtained by a global optimization procedure, and they seem to obey SLE. Thus, the reason for the failure of the SLE property for MWP is still not totally clear to us.

ACKNOWLEDGMENTS

We thank P. Grassberger and A. A. Saberi for valuable discussions. C.N. acknowledges financial support from the Deutsche Forschungsgemeinschaft (DFG) under Grant No. AS 136/2-1. O.M. acknowledges financial support from the DFG under Grant No. HA 3169/3-1. The simulations were performed at the HERO cluster of the University of Oldenburg, funded by the DFG (INST 184/108-1 FUGG) and the ministry of Science and Culture (MWK) of the Lower Saxony State, and the GOLEM I Cluster for Scientific Computing both located at the University of Oldenburg (Germany).

[1] D. Stauffer and A. Aharony, *Introduction to Percolation Theory* (Taylor and Francis, London, 1994).
[2] W. Janke and A. M. J. Schakel, Phys. Rev. E **71**, 036703 (2005).
[3] M. Kardar and Y. C. Zhang, Phys. Rev. Lett. **58**, 2087 (1987).
[4] B. Derrida, Physica A **163**, 71 (1990).
[5] P. Grassberger, J. Phys. A **26**, 1023 (1993).

[6] S. V. Buldyrev, S. Havlin, and H. E. Stanley, Phys. Rev. E **73**, 036128 (2006).
[7] F. O. Pfeiffer and H. Rieger, J. Phys.: Condens. Matter **14**, 2361 (2002).
[8] F. O. Pfeiffer and H. Rieger, Phys. Rev. E **67**, 056113 (2003).
[9] T. Vachaspati and A. Vilenkin, Phys. Rev. D **30**, 2036 (1984).
[10] R. J. Scherrer and J. A. Frieman, Phys. Rev. D **33**, 3556 (1986).
[11] H. Hindmarsch and K. Strobl, Nucl. Phys. B **437**, 471 (1995).
[12] M. Cieplak, A. Maritan, and J. R. Banavar, Phys. Rev. Lett. **72**, 2320 (1994).
[13] O. Melchert and A. K. Hartmann, Phys. Rev. B **76**, 174411 (2007).
[14] K. Schwarz, A. Karrenbauer, G. Schehr, and H. Rieger, J. Stat. Mech. (2009) P08022.
[15] D. Stauffer, Phys. Rep. **54**, 1 (1979).
[16] A. Allega, L. A. Fernández, and A. Tarancón, Nucl. Phys. B **332**, 760 (1990).
[17] D. Austin, E. J. Copeland, and R. J. Rivers, Phys. Rev. D **49**, 4089 (1994).
[18] J. Cardy, Ann. Phys. (NY) **318**, 81 (2005), Note: Summary is available at http://www.papercore.org/Cardy2005.
[19] W. Kager and B. Nienhuis, J. Stat. Phys. **115**, 1149 (2004).
[20] M. Bauer and D. Bernard, Comm. Math. Phys. **239**, 493 (2003).
[21] J. L. Jacobsen, P. Le Doussal, M. Picco, R. Santachiara, and K. J. Wiese, Phys. Rev. Lett. **102**, 070601 (2009).
[22] M. E. J. Newman and G. T. Barkema, *Monte Carlo Methods in Statistical Physics* (Clarendon, Oxford, 1999).
[23] N. Schwartz, A. L. Nazaryev, and S. Havlin, Phys. Rev. E **58**, 7642 (1998).
[24] H. Rieger, J. Phys. A **36**, 11095 (2003).
[25] O. Melchert and A. K. Hartmann, New. J. Phys. **10**, 043039 (2008).
[26] O. Melchert, Ph.D. thesis, University of Oldenburg, 2009.
[27] O. Melchert and A. K. Hartmann, Comput. Phys. Commun. **182**, 1828 (2011).
[28] L. Apolo, O. Melchert, and A. K. Hartmann, Phys. Rev. E **79**, 031103 (2009).
[29] O. Melchert, L. Apolo, and A. K. Hartmann, Phys. Rev. E **81**, 051108 (2010).
[30] O. Melchert and A. K. Hartmann, Eur. Phys. J. B **80**, 155 (2011).
[31] O. Melchert, A. K. Hartmann, and M. Mézard, Phys. Rev. E **84**, 041106 (2011).
[32] O. Schramm, Israel J. Math. **118**, 221 (2000).
[33] D. Bernard, G. Boffetta, A. Celani, and G. Falkovich, Nat. Phys. **2**, 124 (2006).
[34] S. Smirnov, Eur. Math. Soc. **2**, 1421 (2006).
[35] S. Smirnov, Comptes Rendus Acad. Sci. Paris, Math. **333**, 239 (2001).
[36] C. Amoruso, A. K. Hartmann, M. B. Hastings, and M. A. Moore, Phys. Rev. Lett. **97**, 267202 (2006).
[37] *Conformal Invariance: an Introduction to Loops, Interfaces and Stochastic Loewner Evolution*, edited by M. Henkel and D. Karevski (Springer, New York, 2012).
[38] *Papercore* is a free and open access database for summaries of scientific (currently mainly physics) papers, http://www.papercore.org/.
[39] A. Cayley, Crelle's J. **32**, 119 (1846).
[40] R. K. Ahuja, T. L. Magnanti, and J. B. Orlin, *Network Flows: Theory, Algorithms, and Applications* (Prentice Hall, New York, 1993).
[41] W. Cook and A. Rohe, INFORMS J. Computing **11**, 138 (1999).
[42] A. K. Hartmann and H. Rieger, *Optimization Algorithms in Physics* (Wiley-VCH, Weinheim, Germany, 2001).
[43] For the calculation of minimum-weighted perfect matchings we use Cook and Rohes BLOSSOM4 extension to the Concorde library, http://www2.isye.gatech.edu/∼wcook/blossom4/.
[44] V. Beffara, Ann. Probab. **32**, 2606 (2004).
[45] V. Beffara, Ann. Probab. **36**, 1421 (2008).
[46] S. V. Buldyrev, S. Havlin, E. López, and H. E. Stanley, Phys. Rev. E **70**, 035102(R) (2004).
[47] S. Risau-Gusman and F. Romá, Phys. Rev. B **77**, 134435 (2008).
[48] M. Picco and R. Santachiara, Phys. Rev. Lett. **100**, 015704 (2008).
[49] C. Chatelain, J. Stat. Mech. (2010) P08004.
[50] D. Bernard, P. Le Doussal, and A. A. Middleton, Phys. Rev. B **76**, 020403(R) (2007).
[51] O. Schramm, Elect. Comm. in Probab. **6**, 115 (2001).
[52] A. Gamsa and J. Cardy, J. Stat. Mech. (2007) P08020.
[53] A. K. Hartmann, *Practical Guide to Computer Simulations* (World Scientific, Singapore, 2009).
[54] B. Duplantier and H. Saleur, Phys. Rev. Lett. **60**, 2343 (1988).
[55] B. Wieland and D. B. Wilson, Phys. Rev. E **68**, 056101 (2003).
[56] A. A. Saberi and S. Rouhani, Phys. Rev. E **79**, 036102 (2009).
[57] A. A. Saberi, H. Dashti-Naserabadi, and S. Rouhani, Phys. Rev. E **82**, 020101(R) (2010).